XL CILAMCE
IBERO-LATIN AMERICAN CONGRESS ON COMPUTATIONAL METHODS IN ENGINEERING
NOVEMBER 11-14, 2019
Praiamar Natal Hotel & Convention Natal, RN-BRAZIL

FLUID-STRUCTURE INTERACTION COMPUTATION WITH MULTI-SCALE OVERLAPPING MESHES

Rodolfo A. K. Sanches
University of São Paulo
Jeferson W. D. Fernandes
University of São Paulo
Kenji Takizawa
Waseda University
Tayfun E. Tezduyar
Rice University

Abstract

Many fluid–structure interaction (FSI) and other moving-boundary flow problems involve localized effects within a larger flow domain, such as boundary layers near a flexible structure. Accurate and realistic computational analysis of such problems requires that the local flow behavior is properly represented by the methods, with sufficient computational flexibility and reasonable computing cost. There are basically two approaches: interface-tracking (moving mesh) and interface-capturing (nonmoving mesh) methods. In the first approach, arbitrary Lagrangian–Eulerian or space–time methods are employed to allow the fluid mesh to deform and follow the moving structure. Moving-mesh methods are more suitable when there are no topological changes (TC) in the flow domain, such as contact between solid surfaces, demanding sophiscated techniques to take TC into account. In the second approach, immersed-boundary methods are used to allow the structure to move over a mesh that is not following the interface. This approach is seen by most as the practical way in flow problems with TC. However, the approach might involve numerical problems due to the conditions imposed at the immersed boundary and quite often will not have sufficient mesh resolution to accurately represent the boundary layers. We propose a method with overlapping multiscale meshes, combining a global mesh that is constructed over the entire flow domain and does not follow the structure and a finer and deforming local mesh that follows the structure. For coupling the local and global meshes, a Function-space Blending Technique is developed, which is based on local modification and superposition of the local and global bases inside a defined overlapping region. The method is more flexible than the traditional moving-mesh methods, as the remeshing will be less frequent and, when it happens, will be applied only to a small local mesh. At the same time, this method overcomes the shortcomings of the nonmoving-mesh methods in boundary-layer representation.

Keywords: Fluid-structure interaction; overlapping meshes; multiscale analysis.

1 Introduction

Most of fem formulations for simulating moving boundary flows, fit into one of this 2 different classes: interface-tracking (moving mesh) or interface-capturing (nonmoving mesh).

In the interface-tracking methods, formulations that allow the fluid mesh to deform arbitrarily, like the arbitrary Lagrangian–Eulerian (ALE) [1] or space–time methods [2, 3], are employed to allow the computational fluid domain to follow structural movements. Those are very robust methods, however, will demand additional techniques to deal with problems with topological changes (TC) in the fluid domain, or even some problems with very large deformations of the fluid domain at a point that it is not impossible for the fluid mesh to accommodate the domain deformation.

In the second approach, immersed-boundary methods (see a good review in Mittal and Iaccarino [4]) are used to allow the structure to move inside a fixed fluid mesh. This approach is seen by most as the practical way in flow problems with TC. However, it might involve numerical problems due to the conditions imposed at the immersed boundary and, for some situations, it is not impossible to use adaptive refinement in order to represent properly boundary layers or discontinuities that may appear very close to the moving fluid-structure interface.

In the point of view of fluid mechanics, one can classify the problem of a structure moving inside a much larger domain as a localized problem. Getting an accurate and realistic computational analysis of these problems requires that the local mechanics behavior is properly represented with methods with sufficient computational flexibility and reasonable computing cost. This allows us to deal with such problem as a two-scale problem, with a local model close to the structure, coupled to a global model.

Several authors have conducted studies aiming to enhance a global FEM model resolution regarding localized effects, covering a large range of mechanical problems. Among these studies, there is one set of methods that suggest to work both on macro- and micro-levels, with micro-fields correcting the macro-ones (see [5, 6]).

In the context of unsteady flow problems with two-fluid and fluid-free surface interfaces, [7] and [8] introduce the Enhanced-Discretization Interface-Capturing Technique (EDICT). In such method, the fem function spaces are based on enhanced discretization at and near the interface. Initially a subset of the elements in the base mesh, Mesh-1, is identified by those elements at and near the interface. A more refined mesh, Mesh-2, is constructed by patching together second-level meshes generated over each element in this subset. Although the discretization is enhanced to capture the interface, meshes do not fit to the interface of the discontinuity.

In a general context, Dhia [9], Dhia and Rateau [10], introduce the Arlequin method, which consists in the superposition of models in defined overlapping region. In this method, the models are glued to each other in a subzone of overlapping region called glue zone, where a Lagrange Multiplier field is defined in order to consolidate local and global models, introducing extra unknowns to the problem.

In this work, we introduce in the context of FSI, a mesh blending method that enables us to use a local fluid mesh overlapping with a global one. The local mesh is conform to the structure and deforms tracking the structural motion, while the global mesh is fixed. This allows us to combine advantages of interface-tracking and interface-capturing methods. The presence of a fine discretization close to the structure is ensured, in order to represent local effects, and at the same time that, by deforming only the local mesh, a larger scale of displacements is tolerated compared to the standard interface-tracking methods. In cases of topology change, like structural contact problems, mesh reconstruction applies only in the local mesh.

We perform the mesh blending by modifying the local and global basis function spaces in the overlap region and adding them keeping the partition of unity. This method has the advantage over other overlapping meshes methods of no need for Lagrange multipliers, penalty parameters or other method to glue local and global models.

We test the blending method on 1D and 2D steady state problems, and then, apply it to 2D fluid-structure interaction problem. We consider an implicit stabilized fem formulation for 2D analysis of incompressible flows, with ALE description in the local model, coupled to a large displacement 2D

frame dynamics solver with positional formulation [11, 12] with isogeometric discretization.

2 Mesh blending technique

Let us consider the physical domain Ω composed by the union of a global domain Ω_G and containing a local domain Ω_L with the region of localized effects inside it, so that $\Omega = \Omega_G \cup \Omega_L$.

The physical boundary of the domain Ω can be divided into the portion related to the global domain $\Gamma_G = (\Gamma_G)_g \cup (\Gamma_G)_h$ and the portion related to the local domain $\Gamma_L = (\Gamma_L)_g \cup (\Gamma_L)_h$, where subscripts g and h identify Dirichlet and the Neummann boundaries respectively. Notice that Γ_G or Γ_L may not exist or present only Dirichlet or only Neummann boundary conditions.

We also deffine non-physical boundaries $(\Gamma_G)_B$ and $(\Gamma_L)_B$ only to limit global and local domains inside the physical domain (see figure 1).

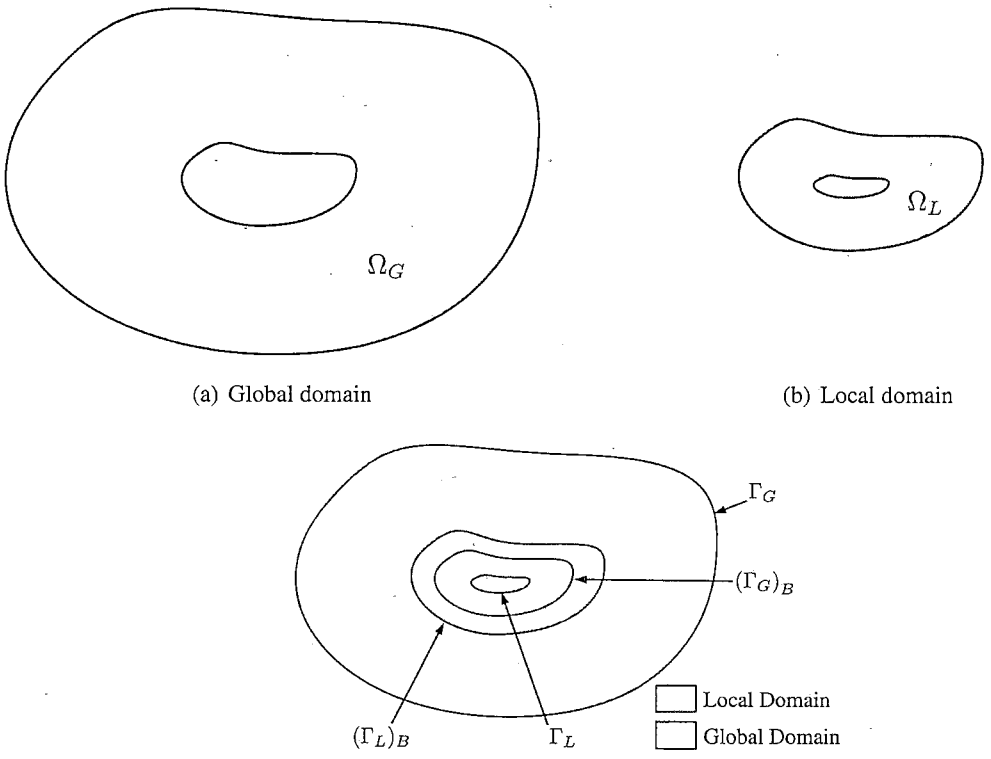

(a) Global domain

(b) Local domain

(c) Physical domain

Figure 1. Physical domain decomposition

We allow Ω_G and Ω_L to overlap defining a blending region $\Omega_B = \Omega_G \cap \Omega_L$, bounded by $(\Gamma_G)_B$ and $(\Gamma_L)_B$. This method is built over the assumption that this region is larger than zero and not larger than the local domain.

Considering that initially independent tests and trials spaces are defined for the global and for the local domains, so that the test functions are given by: $w_G(\mathbf{x}) \in \mathcal{V}_G$ and $w_L(\mathbf{x}) \in \mathcal{V}_L$, and the trial functions are given by: $u_G(\mathbf{x}) \in \mathcal{S}_G$ and $u_L(\mathbf{x}) \in \mathcal{S}_L$.

The direct union of the trial and test spaces from both models in order to provide the function spaces for the physical domain Ω will result into inadequate function spaces which do not hold the unity partition property. Moreover, it is necessary a specific criteria to pic test and trial functions, which are not necessarily limited to the blending domain.

It is done by making a weighted addition of the test and trial function (blending), so that the new

test and trial functions are givenby:

$$u(\mathbf{x}) = b(\mathbf{x})u_G(\mathbf{x}) + (1 - b(\mathbf{x}))u_L(\mathbf{x}) \tag{1}$$

and

$$w(\mathbf{x}) = b(\mathbf{x})w_G(\mathbf{x}) + (1 - b(\mathbf{x}))w_L(\mathbf{x}) \tag{2}$$

where b is called blending function, with value 1 over the global domain free zone ($\Omega_G - \Omega_L$), 0 over the local domain free zone ($\Omega_L - \Omega_G$), and with a specially designed smooth transition over Ω_B.

The initial trial and test spaces remain unchanged in the free zones, however, in the blending region, they are modified, so that for the blended physical domain Ω we define new enriched spaces $\mathcal{S}_{enr}$ containing u and $\mathcal{V}_{enr}$ containing w, so that the solution of a boundary value problem can now be defined as: find $u(\mathbf{x}) \in \mathcal{S}_{enr}$ so that

$$B(u, w) = F(w), \ \forall w \in \mathcal{V}_{enr}, \tag{3}$$

or by: find $u_L(\mathbf{x}) \in \mathcal{S}_L$ and $u_G(\mathbf{x}) \in \mathcal{S}_G$ such that, for a specially chosen function b,

$$\begin{aligned} B(bu_G + (1-b)u_L, bw_G + (1-b)w_L) = F(bw_G + (1-b)w_L), \\ \forall w_L \in \mathcal{V}_L \text{ and } \forall w_G \in \mathcal{V}_G. \end{aligned} \tag{4}$$

In the equations above $B(\bullet, \bullet)$ and $F(\bullet)$ are respectively a bilinear and linear functional operators from $\mathcal{V}_{enr} \times \mathcal{S}_{enr}$ to $\mathbb{R}$.

In order to get the discrete problem based on the finite element technique, we simply multiply the shape functions $\mathbf{N}_G(\mathbf{x})$ of the global discretization by $b(\mathbf{x})$ and the shape functions $\mathbf{N}_L$ of the local discretization by $(1 - b(\mathbf{x}))$, so that the trial solution is given by:

$$u^h(\mathbf{x}) = \sum_{A=1}^{(n_{np})_G} (u_G)_A b(\mathbf{x})(N_G)_A(\mathbf{x}) + \sum_{A=1}^{(n_{np})_L} (u_L)_A(1 - b(\mathbf{x}))(N_L)_A(\mathbf{x}). \tag{5}$$

where $(n_{np})_G$ and $(n_{np})_L$ are the number of shape functions respectively of the global and of the local discretizations. One can see that the problem is now equivalent to solve a standard fem problem with new shape functions obtained by modifying the ones already existing for each domain.

Such procedure, in order to lead to a single solution, requires the modified basis functions $b(\mathbf{x})\mathbf{N}_G(\mathbf{x})$ and $(1 - b(\mathbf{x}))\mathbf{N}_L(\mathbf{x})$ to be linearly independent over Ω_B. This requires $b(\mathbf{x})$ to be chosen in order to ensure such linearly independence. However, it is important to mention that iterative solution methods may lead to the desired solution (specially for dynamic problems, where a good initial guess is well defined) even with linearly dependency.

2.1 Blending function definition

In order to keep the method practical, we consider that the global mesh has the size of the domain Ω and the boundary $(\Gamma_G)_B$ is latter defined based on the shape of the local model. The global elements and nodes with no physical support or very small support after the blending process are deactivated from the analysis.

In order to define b, we first define X_L as the signed distance function from the boundary $(\Gamma_L)_B$ (external boundary of the local domain), considered positive inside the local domain and negative outside. The next step is to define a signed distance X_G to $(\Gamma_G)_B$, positive if the point is inside Ω_G and negative if the point is outside. The blending domain Ω_B is defined by the points where both signed distance are positive. The blending function can now be evaluated as a function of X_L and X_G.

Considering shape functions of order n, in the 1D case, we need b to be a function of order $n + 1$ in order to provide $2(n + 1)$ shape functions of order $2n + 1$ over the blending zone.

We first define the parameter $\delta(\mathbf{x}) = X_L(\mathbf{x}) + X_G(\mathbf{x})$. This parameter coincides with the blending domain thickness when $(\Gamma_G)_B$ and $(\Gamma_L)_B$ are parallel.

In this work, we apply the same Idea for the 2D case considering quadratic shape functions, so that the blending function $b(\mathbf{x})$ is cubic with X_L, given by:

$$b(\mathbf{x}) = \begin{cases} 2\left(\frac{X_L(\mathbf{x})}{\delta(\mathbf{x})}\right)^3 - 3\left(\frac{X_L(\mathbf{x})}{\delta(\mathbf{x})}\right)^2 + 1 & \text{if } X_G(\mathbf{x}) > 0 \text{ and } X_L(\mathbf{x}) > 0 \\ 1 \quad \text{if } X_L(\mathbf{x}) \leq 0 \\ 0 \quad \text{if } X_G(\mathbf{x}) \leq 0 \end{cases} \tag{6}$$

Considering quadratic shape functions, the proposed method will provide a basis of degree $n = 5$ over the blending region, with 6 nonzero shape functions at any point. The size of the domain Ω_B also affects the precision of the solution. The region Ω_B is a region with higher order shape functions and more nodal points, so that the quality of the numerical solution is increased when Ω_B increases. However increasing Ω_B may result in shape functions much smaller than others, damaging the precision of the method as one can see in the numerical tests of section 3.

The size of the blending region affects the precision of the solution. At the same time that the blending domain has a more accurate basis, it can also contain shape functions with very small support in the physical domain, making the system ill-conditioned as Ω_B increases.

Figure 2 illustrates the process applied to a 1D discretization with quadratic shape functions.

3 Preliminary 1D tests

In order to study the numerical characteristics or the proposed method, we start by considering a 1D elastic bar of length l, clamped at both ends, with Young's modulus $E = 1$ and cross section area $S = 1$, under the axial distributed load $f = cos(\pi x/l)$. The governing differential equation is given by:

$$\frac{d^2\,u}{d\,x^2} - f = 0 \;\; \Omega = (a, b) \tag{7}$$

with $u(a) = 0$ and $u(b) = 0$, where a and b are respectively the left and the right boundary position. Considering $a = 0$ and $b = l$.

Convergence with fixed overlap length

In order to solve this problem we use the same discretization for local and global model, with size l. Initially we set the blending domain size equal to the length ($\Omega_B = \Omega_G = \Omega_L$) implying $\delta = l$. The size of the elements is then modified equally for both models at same time. Four different element sizes are considered: $h = l, l/2, l/3, l/6$ and $l/12$.

One can notice from figure 3 that the problem starts converging with the same convergence rate as expected for a 5^{th} degree basis, however it lowers the convergence rate by about one order as the elements get smaller. It is explained by the presence of shape functions with small support when refining the mesh and keeping the blending domain size constant.

Convergence analysis for $\delta = h$

Following, we fix the blending domain length to the size of one element and perform a convergence analysis expecting to get no less than the $O(h)^3$ for the error in L_2 norm and less the $O(h)^2$ for the error in H_1 semi-norm. It is confirmed by the results in figure 4.

These preliminary results serve as a guideline for expanding the method to higher dimensions.

4 Incompressible fluid flow modeling

In order to model Navier-Stokes equations for incompressible flow, we use the SUPG/PSPG (Streamline Upwind Petrov Galerkin/Pressure Stabilization Petrov Galerkin) formulation of the finite element

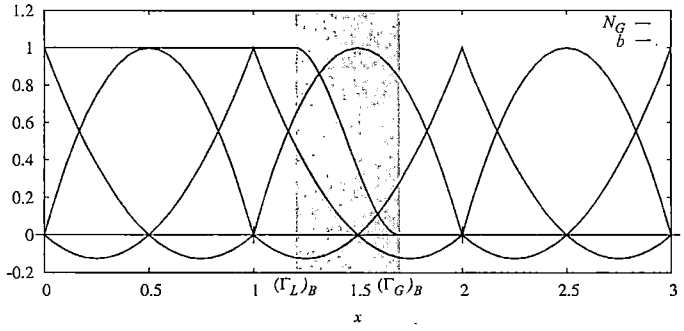

(a) Global Model

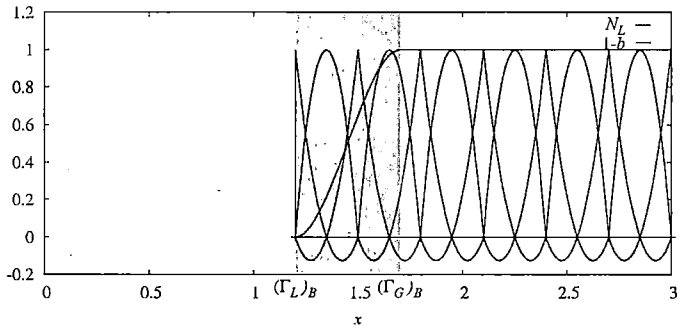

(b) Local Model

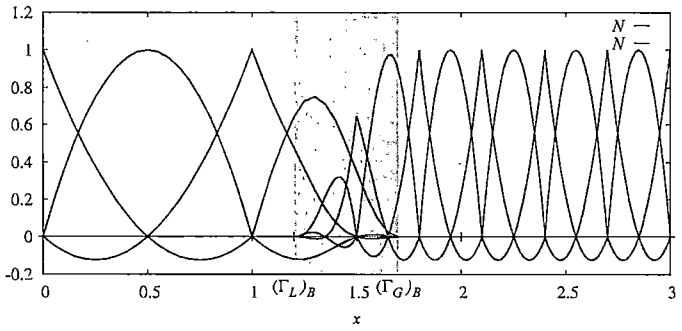

(c) Blended Model

Figure 2. 1D Blending.

method as described by [13], with time marching integration based on the implicit trapezoidal rule (second order accurate).

The stabilized weak form of the governing equations in ALE description is then given by:

$$\begin{aligned}\int_\Omega \mathbf{w}^h \cdot \rho\left(\frac{\partial \mathbf{u}^h}{\partial t} + (\mathbf{u}^h - \mathbf{v}^h)\cdot\nabla\mathbf{u}^h - \mathbf{f}^h\right) d\Omega + \int_\Omega \boldsymbol{\varepsilon}\left(\mathbf{w}^h\right) : \boldsymbol{\sigma}\left(\mathbf{u}^h, p^h\right) d\Omega \\ - \int_{\Gamma_\mathrm{h}} \mathbf{w}^h \cdot \mathbf{h}^h d\Gamma \\ + \sum_{e=1}^{n_\mathrm{el}} \int_\Omega^e \tau_\mathrm{SUPG}\left((\mathbf{u}^h - \mathbf{v}^h)\cdot\nabla\mathbf{w}^h\right)\cdot\mathbf{r}_\mathrm{M}\left(\mathbf{u}^h, p^h\right) d\Omega \\ + \sum_{e=1}^{n_\mathrm{el}} \int_\Omega^e \nu_\mathrm{LSIC}\nabla\cdot\mathbf{w}^h r_\mathrm{C}\left(\mathbf{u}^h\right) d\Omega = 0\end{aligned} \tag{8}$$

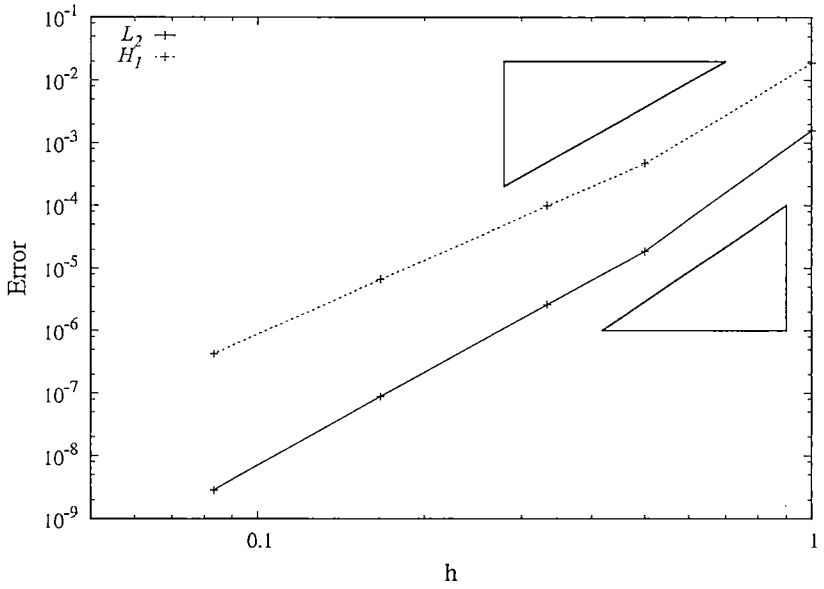

Figure 3. Convergence for fixed overlap lenght δ.

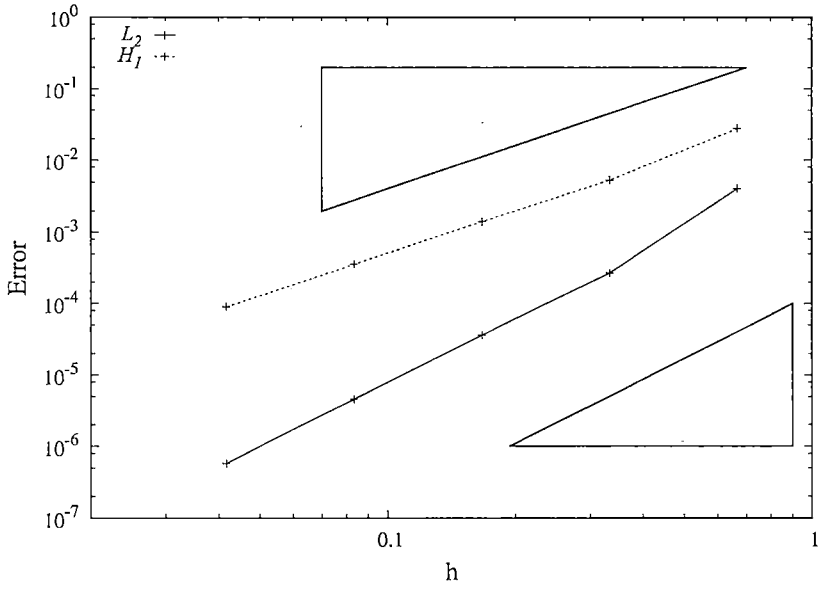

Figure 4. Convergence with overlap length $\delta = h$.

and

$$\int_{\Omega} q^h \nabla \cdot \mathbf{u}^h d\Omega + \sum_{e=1}^{n_{\text{el}}} \int_{\Omega}^{e} \tau_{\text{PSPG}} \left(\frac{\nabla q^h}{\rho} \right) \cdot \mathbf{r}_{\text{M}} \left(\mathbf{u}^h, p^h \right) d\Omega, \tag{9}$$

where $\mathbf{w}^h$ is the momentum equation test function vector, ρ is the fluid density, $\mathbf{u}^h$ is the interpolated velocity vector, $\mathbf{v}^h$ is the mesh velocity, $\mathbf{f}^h$ is the interpolated body forces vector, $\boldsymbol{\varepsilon}$ is the infinitesimal strain operator, p^h is the interpolated pressure, $\boldsymbol{\sigma}$ is the Cauchy stress tensor, $\mathbf{h}^h$ is the traction vector at Neumann boundary, $\mathbf{r}_{\text{M}}$ is the residua of momentum equation, r_{C} is the residua of continuity equation and q is the continuity equation test function.

The stabilizing parameters stabilizing parameters τ_{PSPG}, τ_{SUPG} and ν_{LSIC} are computed according to Takizawa et al. [14]. One important point regarding the use of the mesh blending procedure for the stabilized formulation of fluid dynamics is the evaluation of the stabilizing parameters. The stabilizing parameters for both, convection and pressure, are based on a scale length, which is taken as measure

of the element length in the critical direction. The choice of optimal parameters in the blending zone is still to be investigated, however, in this paper we chose to compute two parameters, $(\tau_{\text{SUPG}})_L$ and $(\tau_{\text{SUPG}})_G$, respectively for local and global meshes, considering their initial shape functions, and then such parameters are blended by:

$$\tau_{\text{SUPG}}(\mathbf{x}) = b(\tau_{\text{SUPG}})_G + (1-b)(\tau_{\text{SUPG}})_L. \tag{10}$$

4.1 Local-mesh dynamic deformation

In the blended method, considering a moving local-domain, Eq. 8 can be applied directly to the free global domain, considering $\mathbf{v}^h = 0$, and to the free local domain, where $\mathbf{v}^h$ is the computed local mesh velocity. However, a deeper analysis is necessary in the blending region in order to allow only the local basis functions to move. When computing material time derivatives, one need to take into account the shape functions change in time.

In order to deform the local mesh, we apply a Laplacian smoothing for displacements, constraining displacements at fluid/structure interface to the structural displacements, according to Fernandes et al. [15].

4.2 Fixed domain test - Driven cavity incompressible flow

We consider a square cavity with non-dimensional sides of length $l = 1$, with prescribed horizontal velocity at the top $u = 1$. The walls are considered to be no-slip and the fluid viscosity is changed in order to get different Reynolds Numbers.

Five different meshes are used in this simulation, two for global models, being one unstructured (mesh a) and the other structured, and three for local models as shown in Fig. 5. We first use mesh a to get a reference solution and in the sequence local and global meshes are combined in order to test mesh blending technique. We employed 6 nodes triangular finite elements with quadratic Lagrange polynomial shape functions

One can see from Fig. 6, where the horizontal velocity is depicted along the central vertical axe, that the proposed method works as expected. The use of the mesh blending technique for enriching the discretization near the walls clearly give a more accurate representation of the problem, as seen in Figs. 7 and 8.

Moving boundary test - 2D propeller inside a cavity

In this example we consider a 2D propeller inside a cavity unitary non-dimensional length and height, filled with a viscous fluid with non-dimensional viscosity $\mu = 0.1$ and non-dimensional density $\rho = 1$, with boundary conditions and geometry described in fig. 9. The Global mesh has 1238 quadratic triangular elements and 2563 nodes, while the Local mesh has 1626 quadratic triangular elements and 3482 nodes.

A non-dimensional time step $\delta t = 0.01$ is adopted. The propeller is initially at rest and an angular velocity is linearly imposed from $\omega = 0$ at $t = 0$ until $\omega = 1.$ rad/(time unity) at $t = 0.2$, and is then kept constant.

Figure 10 shows pressure and velocity magnitude distribution for some instants and fig. 11 shows the horizontal fluid velocity at the center of the top boundary along time.

5 Fluid-structure interaction with overlapped meshes

We model the fluid as described in section 4, and couple it to a large displacement 2D frame dynamics solver considering Timoshenko/Reissner kinematics in the same way as described by Sanches and Coda [12], but considering isogeometric discretization, with NURBS shape functions, instead of

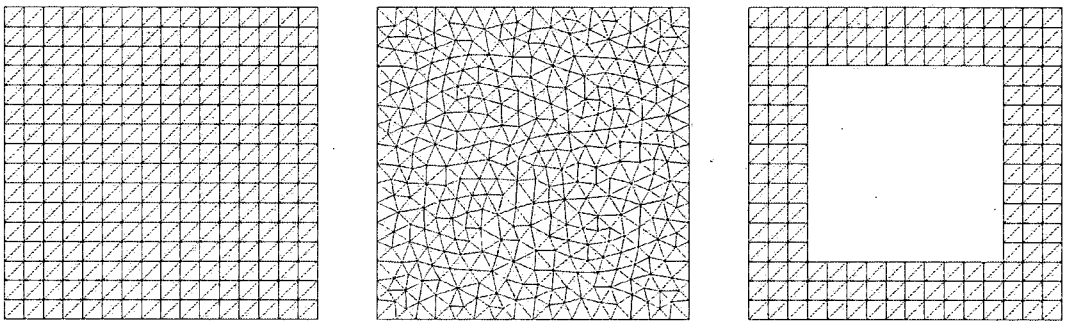

(a) mesh a - global model (b) mesh b - global model (c) mesh c - local model

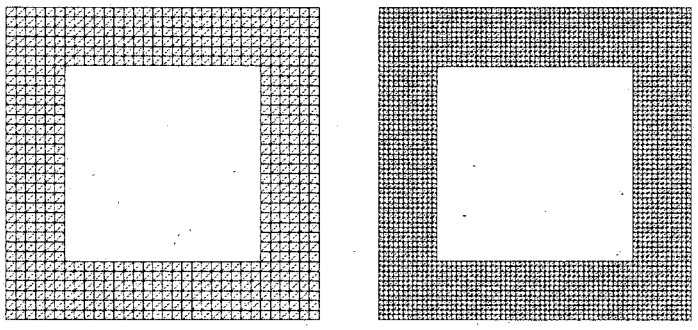

(d) mesh d - local model (e) mesh e - local model

Figure 5. Driven cavity meshes

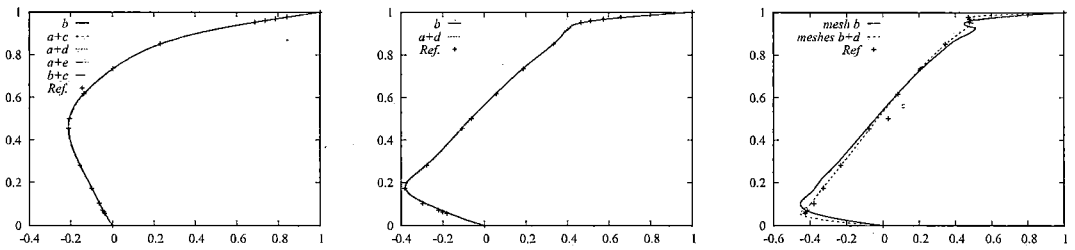

(a) Re 100 (b) Re 1000 (c) Re 10000

Figure 6. Horizontal velocity distribution along y.

finite elements. The block-iterative coupling scheme as described in [16] is adopted in order to solve the coupled problem.

FSI numerical example - Driven cavity with flexible bottom

This example is an extension of the rigid wall cavity problem from item 4.2. In this expansion, explored by many references [17–19], the cavity bottom is replaced by a flexible bar, as illustrated in Fig. 12. Initially, the fluid is at rest and an oscillatory velocity profile given by $\mathbf{u}(t) = [1 - \cos(0.4\pi t),\ 0,\ 0]^T$ is imposed on the cavity upper wall, as well as non-slip condition to the side walls.

Based on the results obtained with the rigid cavity problem, mesh a is chosen for the fluid global model and mesh d for the fluid local model. The bar structure in the bottom is discretized by 32 cells and 35 control points forming one single cubic NURBs patch.

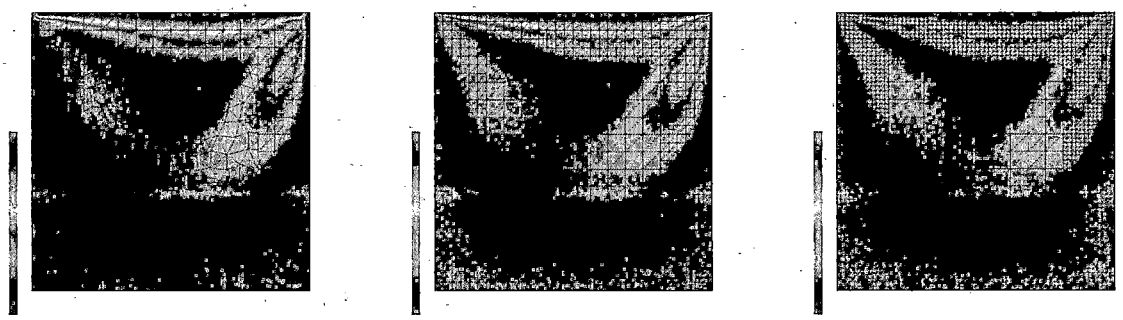

(a) Re 100 Meshes a+c (b) Re 100 Meshes b+d (c) Re 100 Meshes b+d

Figure 7. Non-dimensional velocity magnitude for Re 100 with some different mesh combinations.

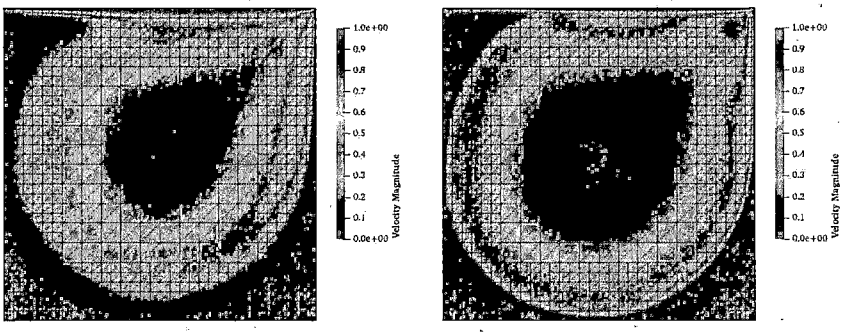

(a) Re 1000 Meshes b+d (b) Re 10000 Meshes b+d

Figure 8. Non-dimensional velocity magnitude for Re 1000 and 10000 with mesh combination b+d.

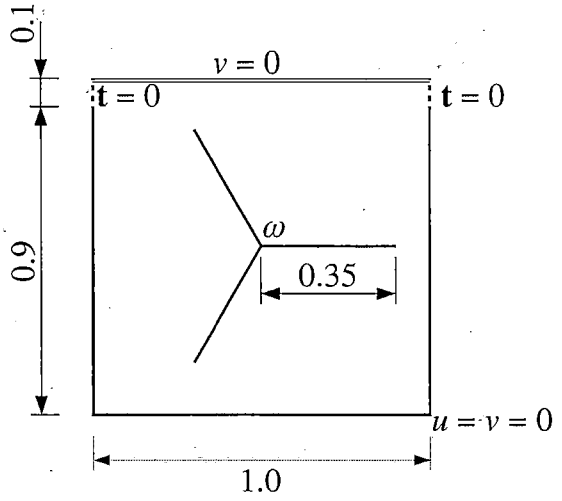

Figure 9. Geometry and boundary conditions for the 2D propeller

In figure 14 we compare the vertical displacement in the center of the bar along time with the solution given by other authors ([17, 20]), showing reasonable agreement, taking into account the different algorithms and elements employed.

Figure 14 shows snapshots of the fluid velocity magnitiude distribution and the vertical component of structural displacements at different instants, where one can see the mesh deformation as well. From

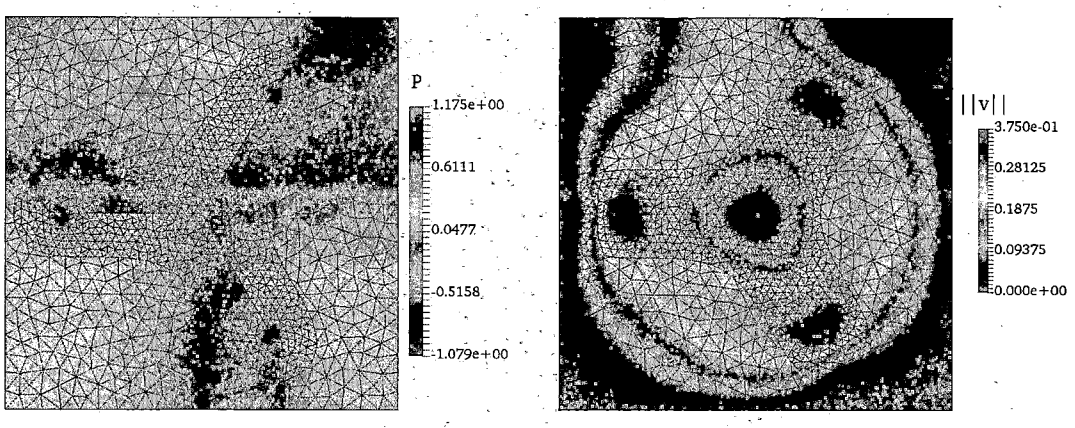

(a) Pressure t = 1.13 s

(b) Velocity t = 1.13 s

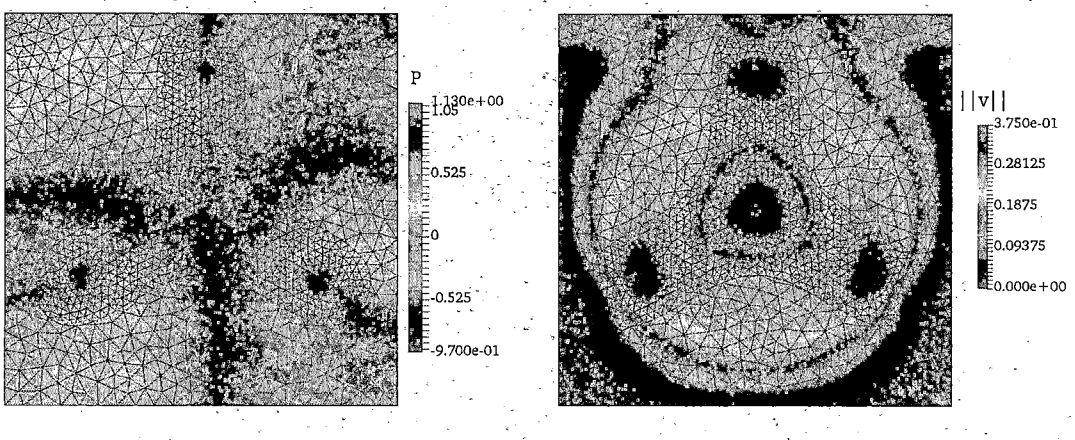

(c) Pressure t = 20.51 s

(d) Velocity t = 20.51 s

Figure 10. Results for 2D Propeller inside a cavity

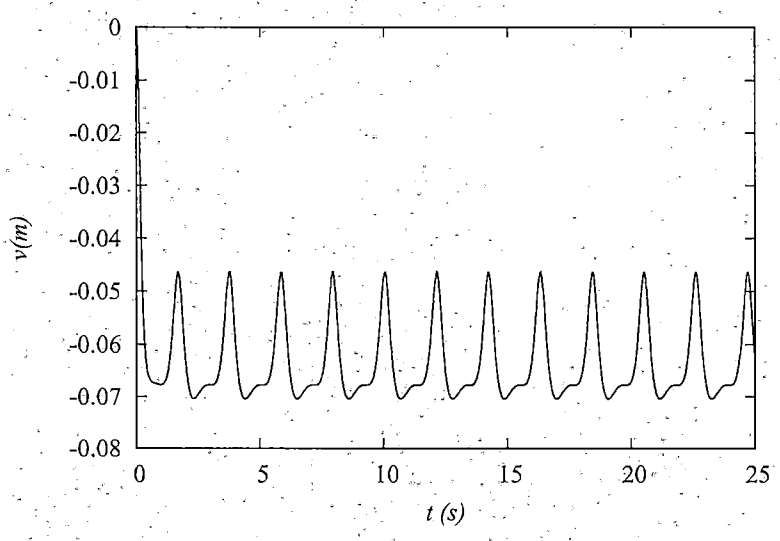

Figure 11. Velocity vs. time at the center of upper boundary

this example it is possible to conclude that the proposed technique is suitable to FSI applications.

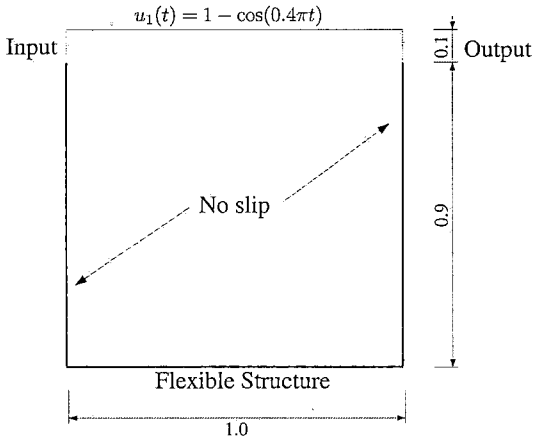

Figure 12. Geometry, boundary conditions and material data of driven cavity with flexible bottom.

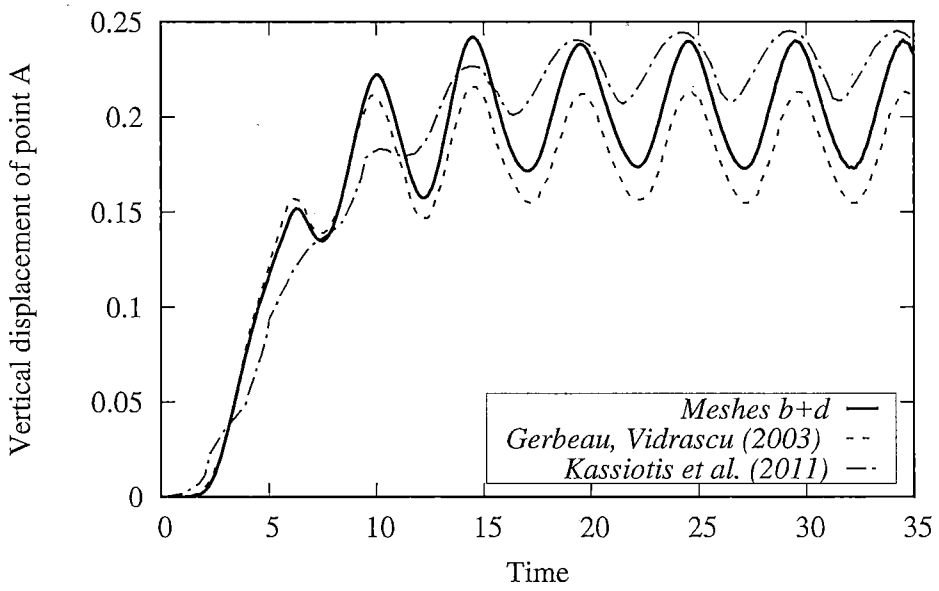

Figure 13. Middle point vertical displacement

6 Conclusion

In this paper, we presented a method for fluid-structure interaction analysis in which a local fluid mesh, coupled to the structure, overlaps a global mesh that discretizes the entire fluid domain. The local mesh is deformable while the global one is fixed, and the bases functions spaces are blended in a subdomain of the overlapping region. The local mesh can be used for enhancing discretization and capturing smaller scale effects, as well to allow larger shape changes to the structure without entangling elements. Another important advantage is that, if topological changes occur, only the local mesh needs to be reconstructed. The function spaces blending method is initially tested in 1D boundary value problems to verify its numerical characteristics. Following, the method is applied to 2D incompressible flow problems with fixed and moving boundaries, and finally, it is coupled to a 2D frame dynamic solver and applied to FSI computation. The results of the numerical example suggests the proposed methodology has great potential as an alternative to FSI problems with large structural shape changes.

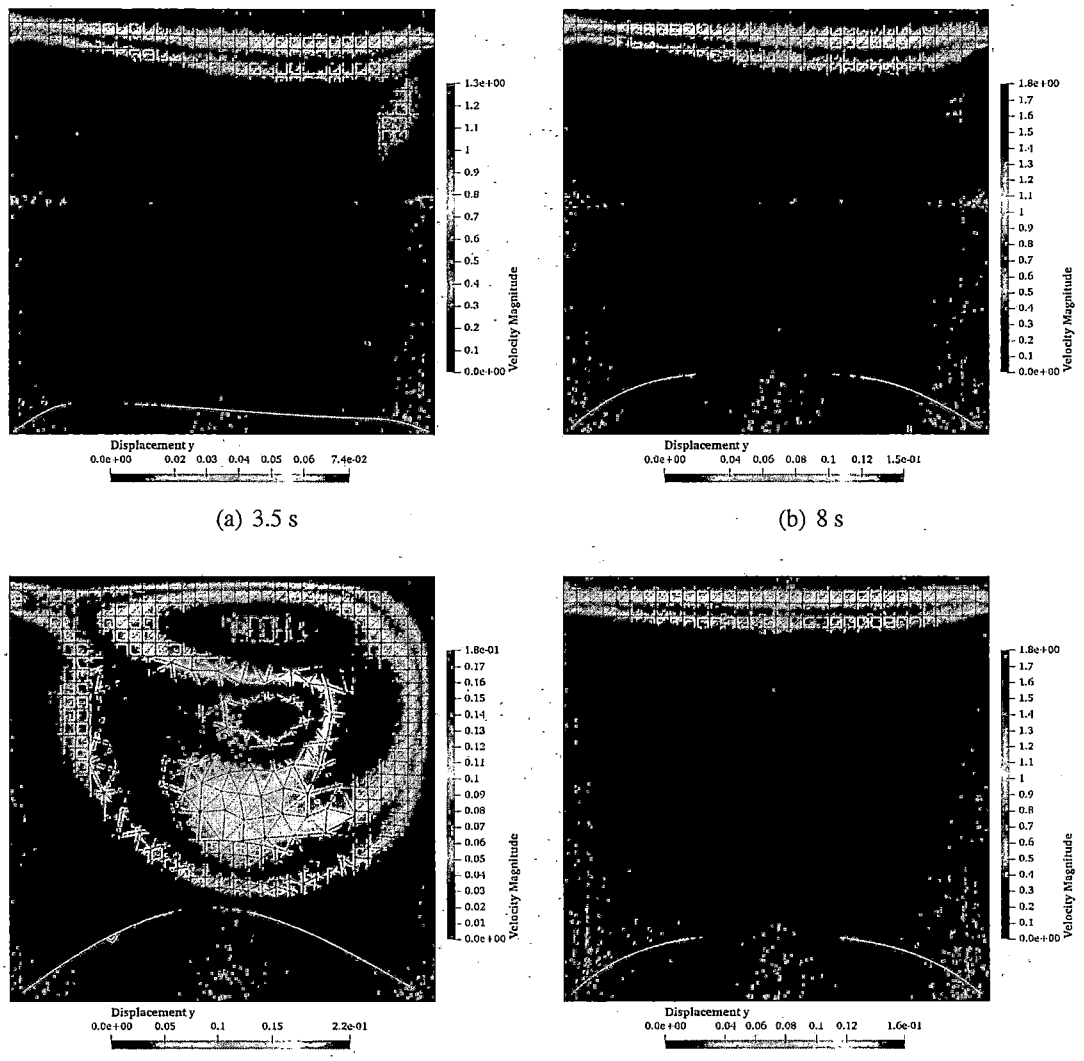

(a) 3.5 s (b) 8 s

(c) 10 s (d) 12 s

Figure 14. Snapshots for the cavity with flexible bottom

Acknowledgements

The authors would like to acknowledge FAPESP, CAPES and CNPq for financial support.

Funding

This study was financed by São Paulo Research Foundation (FAPESP) - Process Number 2016/25520-5, by Brazilian National Council for Research and Technological Development (CNPq) - grant 310482/2016-0 and by *Coordenação de Aperfeiçoamento de Pessoal de Nível Superior - Brasil* (CAPES) - finance code 001.

References

[1] Donea, J., Giuliani, S., & Halleux, J. P., 1982. An arbitrary lagrangian-eulerian finite element method for transient dynamic fluid-structure interactions. *Computer Methods in Applied Mechanics and Engineering*, vol. 33, pp. 689–723.

[2] Tezduyar, T. E., Behr, M., & Liou, J., 1992a. A new strategy for finite element computations involving moving boundaries and interfaces - the deforming-spatial-domain/space-time procedure: I. the concept and the preliminary numerical tests. *Comput. Methods Appl. Mech. Engrg.*, vol. 94, pp. 339–351.

[3] Tezduyar, T. E., Behr, M., Mittal, S., & Liou, J., 1992b. A new strategy for finite element computations involving moving boundaries and interfaces - the deforming-spatial-domain/space-time procedure: II. computation of free-surface flows, two-loquid flows, and flows with drifting cylinders. *Comput. Methods Appl. Mech. Engrg.*, vol. 94, pp. 353–371.

[4] Mittal, R. & Iaccarino, G., 2005. Immersed boundary methods. *Annual Review of Fluid Mechanics*, vol. 37, pp. 239–261. cited By 1024.

[5] Hughes, T. J., Feijóo, G. R., Mazzei, L., & Quincy, J.-B., 1998. Advances in stabilized methods in computational mechanics the variational multiscale method—a paradigm for computational mechanics. *Computer Methods in Applied Mechanics and Engineering*, vol. 166, n. 1, pp. 3 – 24.

[6] Fish, J. & Belsky, V., 1995. Multi-grid method for periodic heterogeneous media part 2: Multiscale modeling and quality control in multidimensional case. *Computer Methods in Applied Mechanics and Engineering*, vol. 126, n. 1, pp. 17 – 38.

[7] Tezduyar, T., Aliabadi, S., & Behr, M., 1998. Enhanced-discretization interface-capturing technique (edict) for computation of unsteady flows with interfaces. *Computer Methods in Applied Mechanics and Engineering*, vol. 155, n. 3, pp. 235 – 248.

[8] Tezduyar, T. E. & Aliabadi, S., 2000. Edict for 3d computation of two-fluid interfaces. *Computer Methods in Applied Mechanics and Engineering*, vol. 190, n. 3, pp. 403 – 410.

[9] Dhia, H. B., 1998. Problèmes mécaniques multi-échelles: la méthode arlequin. *Comptes Rendus de l'Académie des Sciences - Series IIB - Mechanics-Physics-Astronomy*, vol. 326, n. 12, pp. 899 – 904.

[10] Dhia, H. B. & Rateau, G., 2001. Analyse mathématique de la méthode arlequin mixte. *Comptes Rendus de l'Académie des Sciences - Series I - Mathematics*, vol. 332, n. 7, pp. 649 – 654.

[11] Greco, M. & Coda, H. B., 2004. A simple and precise fem formulation for large deflection 2d frame analysis based on position description. *Computer Methods in Applied Mechanics and Engineering*, vol. 193, pp. 3541–3557.

[12] Sanches, R. A. K. & Coda, H. B., 2017. Flexible multibody dynamics finite element formulation applied to structural progressive collapse analysis. *Latin American Journal of Solids and Structures*, vol. 14, n. 1.

[13] Tezduyar, T., Mittal, S., Ray, S., & Shih, R., 1992c. Incompressible flow computations with stabilized bilinear and linear equal-order-interpolation velocity-pressure elements. *Computer Methods in Applied Mechanics and Engineering*, vol. 95, n. 2, pp. 221 – 242.

[14] Takizawa, K., Tezduyar, T. E., & Otoguro, Y., 2018. Stabilization and discontinuity-capturing parameters for space–time flow computations with finite element and isogeometric discretizations. *Computational Mechanics*.

[15] Fernandes, J. W. D., Coda, H. B., & Sanches, R. A. K., 2019. Ale incompressible fluid–shell coupling based on a higher-order auxiliary mesh and positional shell finite element. *Computational Mechanics*, vol. 63, n. 3, pp. 555–569.

[16] Bazilevs, Y., Takizawa, K., & Tezduyar, T., 2013. *Computational Fluid-Structure Interaction: Methods and Applications*. Wiley Series in Computational Mechanics. Wiley.

[17] Gerbeau, J. F. & Vidrascu, M., 2003. A quasi-newton algorithmm based on a reduced model for

fluid-structure interaction problems in blood flows. *ESAIM: Mathematical Modelling and Numerical Analysis*, vol. 37, pp. 631–647.

[18] Förster, C., Wall, W. A., & Ramm, E., 2007. Artificial added mass instabilities in sequential staggered coupling on nonlinear structures and incompressible viscous flows. *Comput. Methods Appl. Mech. Engrg.*, vol. 196, pp. 1278–1293.

[19] Fernández, M. A., Mullaert, J., & Vidrascu, M., 2013. Explicit robin-neumann schemes for the coupling of incompressible fluids with thin-walled structures. *Comput. Methods Appl. Mech. Engrg.*, vol. 267, pp. 566–593.

[20] Kassiotis, C., 2009. *Nonlinear fluid-structure interaction: a partitioned approach and its application through component technology*. Phd thesis, Université Paris-Est, Paris, FR.